Heat Mass Transfer (2017) 53:959–971
DOI 10.1007/s00231-016-1865-7

ORIGINAL

An experimental study of heat transfer and pressure drop characteristics of divergent wavy minichannels using nanofluids

A. Dominic[1] · J. Sarangan[2] · S. Suresh[2] · V. S. Devahdhanush[2]

Received: 14 January 2016 / Accepted: 27 June 2016 / Published online: 18 July 2016

Abstract An experimental investigation was conducted to study the heat transfer and pressure drop characteristics of an array of wavy divergent minichannels and the results were compared with wavy minichannels with constant cross-section. The experiment was conducted in hydro dynamically developed and thermally developing laminar and transient regimes. The minichannel heat sink array consisted of 15 rectangular channels machined on a 30 × 30 mm^2 and 11 mm thick Aluminium substrate. Each minichannel was of 0.9 mm width, 1.8 mm pitch and the depth was varied from 1.3 mm at entrance to 3.3 mm at exit for the divergent channels. DI water and 0.5 and 0.8 % concentrations of Al_2O_3/water nanofluid were used as working fluids. The Reynolds number was varied from 700 to 3300 and the heat flux was maintained at 45 kW/m^2. The heat transfer and pressure drop of these minichannels were analyzed based on the experimental results obtained. It was observed that the heat transfer performance of divergent wavy minichannels was 9 % higher and the pressure drop was 30–38 % lesser than that of the wavy minichannels with constant cross-section, in the laminar regime. Hence, divergent channel flows can be considered one of the better ways to reduce pressure drop. The performance factor of divergent wavy minichannels was 115–126 % for water and 110–113 % for nanofluids.

Keywords Wavy minichannel · Divergent flow passage · Al_2O_3/water nanofluid · Thermally developing flow · Convective heat transfer

List of symbols

A	Amplitude of wavy minichannel (m)
A_s	Surface area (m^2)
C_p	Specific heat capacity (J kg^{-1} K^{-1})
D_h	Hydraulic diameter (m)
DI	De-ionized water
e	Channel height (m)
f	Fanning friction factor (−)
h	Heat transfer coefficient (W m^{-2} K^{-1})
k	Thermal conductivity (W m^{-1} K^{-1})
L	Channel length (m)
m	Mass flow rate (kg s^{-1})
Nu	Nusselt number (−)
P	Pressure (Pa)
Pr	Prandtl number (−)
Q	Power input (W)
Re	Reynolds number (−)
T	Temperature (°C)
u	Channel bulk velocity (m s^{-1})
w_c	Channel width (m)
w_f	Fin width (m)

Greek symbols

ρ	Density (kg/m^3)
μ	Dynamic viscosity (N-s/m^2)
α_c	Minichannel aspect ratio (−)
ΔP	Pressure drop (Pa)

✉ S. Suresh
ssuresh@nitt.edu

A. Dominic
dominicthiru@gmail.com

J. Sarangan
jsarangan@nitt.edu

V. S. Devahdhanush
devahdhanush@hotmail.com

[1] Sona College of Technology, Salem 636 005, Tamilnadu, India

[2] Department of Mechanical Engineering, National Institute of Technology, Tiruchirappalli 620 015, India

ε	Surface roughness (μm)
ϕ	Volume concentration of nanofluids (%)
λ	Wavelength of wavy minichannel (m)

Subscripts

app	Apparent
c	Channel
f	Fluid
fm	Fluid mean
nf	Nanofluid
p	Plenum
s	Surface

1 Introduction

Mini and microchannel heat sinks have found applications in various areas these days. Although the convective heat transfer characteristics of these devices are favourable, there is a major limiting factor in the name of pressure drop [1–7]. The common trend observed is that, if the heat transfer coefficient is increased, the pressure drop across these channels also increases. This requires additional pumping power and stronger flow passages resulting in a higher power requirement and a bulky cooling system [8–10]. Various methods of increasing the heat transfer performance such as the introduction of flow disruptions, reduction of the thermal boundary layer thickness, increment of the velocity gradient near the heater wall, usage of working fluids with better thermophysical properties, etc. have been dealt with by numerous researchers [8–11]. Although the pressure drop increased in most of these cases, the larger increase in heat transfer justified these modifications to be incorporated [3, 6, 7].

Flows which are hydrodynamically fully developed and thermally developing provide very high heat transfer coefficients in the entrance region [1]. In the thermally developing flow regime, the heat transfer coefficient increases with a decrease in the channel size. This was confirmed by the experimental investigation of single-phase water flow through an array of microchannels done by Lee et al. [2]. They also noticed that the mismatches in the boundary and inlet conditions between the microchannel and conventional experiments resulted in the experimental data to be different from that predicted by conventional correlations.

The heat transfer performance of nanofluids has attracted the interests of numerous researchers working in the area of convective heat transfer. A few people have used nanofluids in mini and microchannel heat sinks and obtained positive results. This is evident from the work of Ho et al. [3] who experimentally investigated the forced convective heat transfer of a copper microchannel heat sink with 1 and 2 % vol. Al_2O_3/water nanofluid and showed that heat transfer increased in the case of nanofluids. But the increase in friction factor was small despite the marked increased in dynamic viscosity. A similar investigation by Jung et al. [4] of convective heat transfer coefficient and friction factor of various particle concentrations of Al_2O_3/water nanofluids in rectangular microchannels revealed that the highest convective heat transfer coefficient increase of 32 % was obtained by using 1.8 % nanofluid over water in the laminar flow regime without major friction loss. But in the turbulent regime of Al_2O_3/water nanofluid flow inside a circular aluminium tube, the heat transfer coefficient increased up to a particle concentration of 2 % and the highest heat transfer enhancement was achieved at Re 8000 and 0.5 % concentration [5]. Lee and Mudawar [6] showed that the heat transfer coefficient obtained in the entrance region is higher in the thermally developing region when the concentration of Al_2O_3 nanoparticles is increased, but the enhancement is weaker in the fully developed region. This shows that nanoparticles have an appreciable effect on thermal boundary layer development. Flow induced particle migration in nanofluids also causes the flattening of the velocity profile in the laminar regime. This delays the onset of transition to turbulence. This was confirmed by the experimental investigation of single phase forced convection of Al_2O_3/water nanofluid in a circular minichannel done by Liu et al. [7] for various particle concentrations and Reynolds numbers (600 to 4500). But, they also found that the friction factor and convective heat transfer coefficient of nanofluids in transition region were lower than that of water at similar conditions. But, these differences diminished in the turbulent region. Despite nanofluids having some advantages, it has some disadvantages such as degraded specific heat, higher pressure drop, erosion and clogging of flow passages, long-term fluid settling and higher cost [12].

Wavy channels provide an enhancement in heat transfer over the conventional straight channels because of its geometry and macroscopic mixing. The location of the onset of this heat transfer enhancement moves closer to the entrance of the channel as the flow velocity is increased [13]. The investigation by Nishimura et al. [14] on the flow structure and mass transfer in a wavy macrochannel in the range from laminar to turbulent flow showed that laminar flow had a steady two-dimensional structure, but turbulent flow had a three-dimensional vortical structure. They found that the major reason for the enhancement in heat transfer in these channels is that when the liquid flows past bends and curves, Dean vortices are formed along the flow direction, leading to chaotic advection and enhanced mixing. With increasing Reynolds number, the flow undergoes a transition from a steady state to a periodic one with a single frequency, and subsequently to a quasiperiodic flow with a couple of incommensurate fundamental frequencies. The numerical simulation of the fully developed flow and heat transfer in periodic wavy rectangular

microchannels for various Reynolds number in both the steady and transitional flow regimes by Sui et al. [15] clearly certifies this theory. They also numerically studied the laminar flow and heat transfer of water in three-dimensional wavy microchannels with rectangular cross-section and concluded an increase in the relative waviness along the flow direction results in higher heat transfer performance. Thus, they proposed the variation of the relative waviness along the flow direction depending on the heat transfer performance required at that respective location [16]. Their experimental study [17] of flow friction and heat transfer of DI water flow through sinusoidal rectangular copper microchannels in the Reynolds number range of 300–800 showed that the heat transfer performance of wavy microchannels was much better than that of straight microchannels. At the same time the pressure drop penalty of the present wavy microchannels was much smaller than the heat transfer enhancement. Also, the conjugate simulation results for similar experimental conditions agreed reasonably well with experimental data.

Fluid flow in a divergent straight channel is characterised by the presence of secondary flow co-existing along with the primary axial flow. The experimental investigation of the secondary flow structure and its enhancement on the heat transfer in a bottom wall heated horizontal divergent channel by Yang et al. [18] gives a clear idea of this secondary flow and its interactions. They suggested that secondary flow appearing as mushroom-shaped plumes was associated with vortices in the divergent channel. However, the deceleration of the mainstream caused a thicker heated layer on the heater side, an earlier protrusion of the plumes, and more intense interaction between neighbouring vortices, leading to a larger enhancement of heat transfer than the case of a parallel plate channel. Liu et al. [19] studied the onset of buoyancy-induced secondary flow and heat transfer enhancement in bottom wall heated horizontal divergent and convergent channels and concluded that the destabilisation effect of the decelerated flow in the divergent channel made the onset of the secondary flow and the point of maximum heat transfer to be initiated at an earlier stage, leading to significant variations in the local Nusselt number distribution. This was because of the formation of vortices leading to a complicated flow structure. Shah et al. [20] experimentally investigated the turbulent flow in two-dimensional asymmetric macrochannels subjected to variable adverse (APG) and favourable pressure gradients (FPG). They observed that the mean velocity profiles became ‘more full’ in FPG and ‘less full’ in APG. The lower boundary layer was affected more significantly than the upper boundary layer for APG but the effect was almost similar for FPG. A similar conclusion that divergent channel provides a higher heat transfer coefficient than convergent and constant area ducts for similar mass flow rates, pumping power and pressure drop was provided by Wang et al. [21]. The streamwise deceleration changed the relative thickness of the thermal boundary layer to the hydrodynamic boundary layer. Also, both axial distribution of the local heat transfer coefficient and pressure recovery factor revealed a non-fully developed region in the divergent and convergent channels.

Thus, the above studies reveal the higher heat transfer rate and pressure drop of wavy minichannels over their straight counterparts. The divergent minichannels give a fairly high reduction in pressure drop over the straight minichannels [22]. Hence, to obtain a higher heat transfer rate with a comparatively lower pressure drop, we experimentally studied the single phase flow of DI water and Al_2O_3/water nanofluids in a divergent wavy minichannel heat sink. The effects of Al_2O_3/water nanofluid were also studied in the laminar and transient regimes [11, 12, 23, 24].

2 Formulation of Nanofluid

2.1 Preparation and evaluation of properties

There are two methods to prepare nanofluids viz. a one-step method and a two-step method. Commercial α-phase Al_2O_3 nanoparticles (NanoDur 99.5 %, Alfa Aesar, India) were dispersed in the base fluid (DI water) in two steps to prepare two volume concentrations (0.5 and 0.8 %) of nanofluids. The nominal diameter of the nanoparticles was 40 nm. The SEM image of the nano particles is shown in Fig. 1. The prepared solutions were sonicated by an ultrasonic vibrator (40 kHz, Lark, India) which generated ultrasonic pulses of 180 W at the frequency of 40 kHz. This was done for 60 min to get a uniform and stable nanofluid. The stability of the nanofluids was checked by keeping them in a container for 48 h. There was no sign of significant sedimentation or

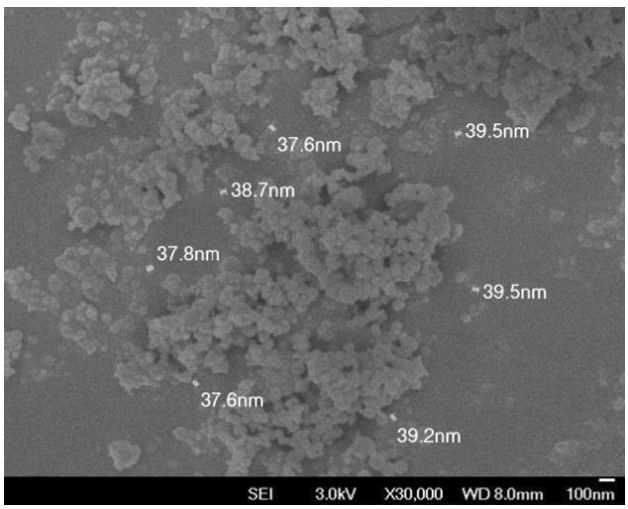

Fig. 1 SEM image of the Al_2O_3 nanoparticles used in the study

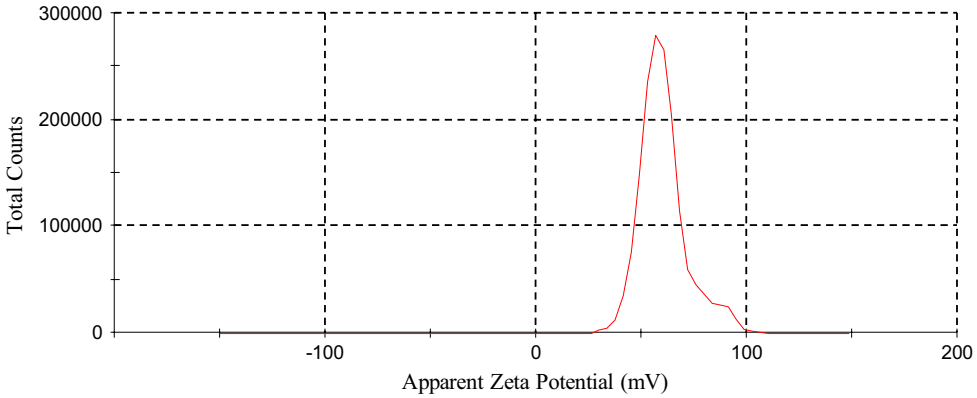

Fig. 2 Zeta potential of the nano particles in 0.8 % Al_2O_3/water nanofluid

settlement in the container. Thermo-physical properties of nanofluids were calculated at the average bulk temperature of the nanofluids and are given below [24].

$\rho_s = 3.6\,\text{g/cc} \quad k_s = 76.5\,\text{W/m-K} \quad C_{p,s} = 880\,\text{J/kg-K}$

The density of Al_2O_3/water nanofluids was determined by using Pak and Cho's Eq. (1) [25].

$$\rho_{nf} = (1-\phi)\rho + \phi\rho_s \tag{1}$$

The specific heat of the nanofluids was calculated by using Xuan and Roetzel's Eq. (2) [26].

$$C_{p,nf} = \frac{(1-\phi)\rho C_p + \phi\rho_s C_{p.s}}{\rho_{nf}} \tag{2}$$

The viscosity of the nanofluids was calculated by using the viscosity correlation (3) proposed by Einstein [27].

$$\mu_{nf} = (1+2.5\phi)\mu \tag{3}$$

The effective thermal conductivity of the nanofluid k_{nf} was calculated by using the Maxwell model [28]. For nanofluids with volume fraction less than unity, Maxwell equation is given by (4),

$$\frac{k_{nf}}{k} = \frac{k_s + 2k + 2\phi(k_s - k)}{k_s + 2k - \phi(k_s - k)} \tag{4}$$

The thermal conductivity and viscosity of the fluids were measured using KD2 Pro Thermal Analyzer and Brookfield Viscometer respectively and compared with the theoretical values, in our previous studies. The difference was just between 1 and 3 % for a maximum volume concentration of 0.008 [29, 30].

While there are some favorable effects of nanofluids on heat transfer performance, it has some adverse effects such as a higher viscosity and density and lower heat capacity. The increment in thermal conductivity, density and viscosity for 0.8 % volume concentration of Al_2O_3/water nanofluids over DI water, were 2.4, 2.08 and 1.99 % respectively; and the degradation of heat capacity was 2.25 % [6].

2.2 Study of stability and size distribution of nanofluid

Nanofluids have some demerits such as clustering, agglomeration and degradation of some thermo-physical properties. These are due to improper methods of preparation and maintenance.

Hence, the stability, size distribution and pH factor of the prepared nanofluids were investigated to ensure its potential features. The stability of the nanofluids [29] was determined by the magnitude (negative or positive) of Zeta potential and pH factor. Zeta potential is the potential difference between the dispersion medium and the liquid layer attached to the nano particles. By a number of measurements of Zeta potential, we can infer if there is agglomeration, dispersion or stabilization. If the value of Zeta potential is around zero, then the particles are at the isoelectric point. The repulsive forces are weak, but attractive van der Waals forces adsorb on the particle surface. So, the colloidal solution is no longer stable and the nano particles settle. If the Zeta potential of the particles is less than 30 mV then dispersion starts. In addition, 30–60 mV of potential shows electrically good stability and more than 60 mV indicates excellent stability. The results of this experiment are shown in the Fig. 2. In the Zeta potential distribution, the Zeta potential was 60.8 mV at a temperature of 25 °C with a Zeta deviation of 9.04 mV. It was given as the apparent Zeta potential (mV), with respect to total counts. It was measured by Zetasizer, Version 7.01(MAL1045544) of Malvern Instruments Ltd (UK).

2.3 Effect of acidity on stability

The pH value measured using a pH meter (Model 111/101, Deep Vision) was around 8. Since the value was close to that of water, it was a stable solution.

2.4 Size distribution of nanofluids

The size of the dispersed individual nanoparticles in the base liquid was measured by Dynamic Light Scattering

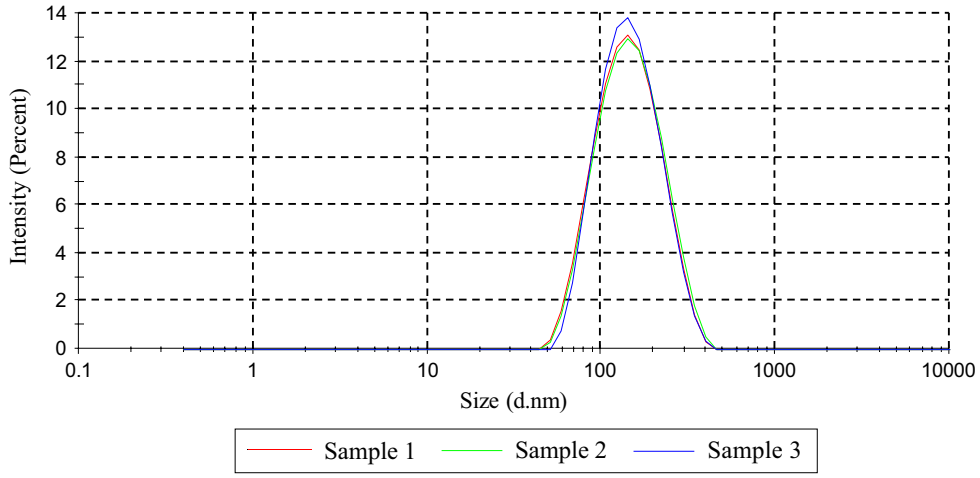

Fig. 3 Size distribution by intensity of nano particles in 0.8 % Al_2O_3/water nanofluid

(using Malvern NanoZS) [31], a technique used for measuring the size of sub-micron sized particles. In this technique, the speed at which the particles are diffusing due to Brownian motion is measured by the rate at which the intensity of the scattered light fluctuates. The intensity of the scattered light fluctuations depends on the size of the particles. The small particles cause the intensity to fluctuate more rapidly than the large ones. And large particles or samples at high concentrations scatter much more light [24].

The average size of the particles in the fluid shown in the size distribution report (Fig. 3), represents the hydrodynamic diameter of nanoparticles. This refers to how a particle diffuses within a fluid. The hydrodynamic diameter or translational diffusion coefficient will depend not only on the size of the particle core but also on any surface structure, concentration and type of ions in the medium. From the image of SEM shown in Fig. 1, the average size of nanoparticles is around 39 nm (the minimum and maximum sizes being 37.6 and 39.5 nm respectively). The average size of the particles in the prepared nanofluid was found to be 130 ± 10 nm as shown in Fig. 3, which was more than the actual size, due to particle agglomeration and clustering. Since the measured size was very closer to the actual size of (39 nm) nano particles, we concluded that the dispersion quality was good and well stable [7, 24].

3 Experimental process

3.1 Experimental setup

The schematic diagram of the experimental setup used in the present investigation is shown in Fig. 4a. The validation of this setup was done for our previous work [11] and the same holds good for this set of experiments too. The flow circuit consisted of the minichannel heat sink assembly, heat exchanger immersed in a water bath, fluid reservoir with a filter and a peristaltic pump with a pulse dampener. The fluid passes through the inlet manifold, inlet plenum, calming section, minichannel heat sink, outlet plenum, outlet manifold and finally to the reservoir through the heat exchanger which was kept in the constant temperature bath. The differential pressure transmitter and concealed thermocouples were connected to both the manifolds to find the pressure drop, inlet and outlet temperatures of the flow. The housing was made up of three polycarbonate plates, as shown in Fig. 4b, c. The top plate contained manifolds with provisions to accommodate thermocouples and a differential pressure transmitter. The middle plate consisted of the inlet and outlet plenums, calming section and provision to hold the minichannel heat sink. The bottom plate contained a plate resistance heater. The housing was made completely leak proof by using Anabond Silicon Red sealant. The housing was kept inside a wooden box with highly insulating glass wool to avoid heat leak.

Figure 5a, b shows the schematic top and side views of the two channel configurations used. The angle of divergence was 3.81°. The entrance and exit depths of the divergent channels was 1.3 and 3.3 mm respectively. Figure 6 shows the photographic view of the wavy minichannel heat sink used. Aluminium was selected as the heat sink material because of a relatively high thermal conductivity (k_{Al} = 204.2 W/m-K), low mass density and high strength. The minichannels were machined by CNC milling on an Aluminium slab of 30 × 30 mm square cross-section and a thickness of 11 mm. 15 parallel constant-cross-section channels of height (e) 1.3 mm, width (w_c) 0.9 mm, hydraulic diameter (d_h) 1.063 mm and aspect ratio (α_c) 1.444 were machined on the slab. But, for the divergent channel configuration, the height

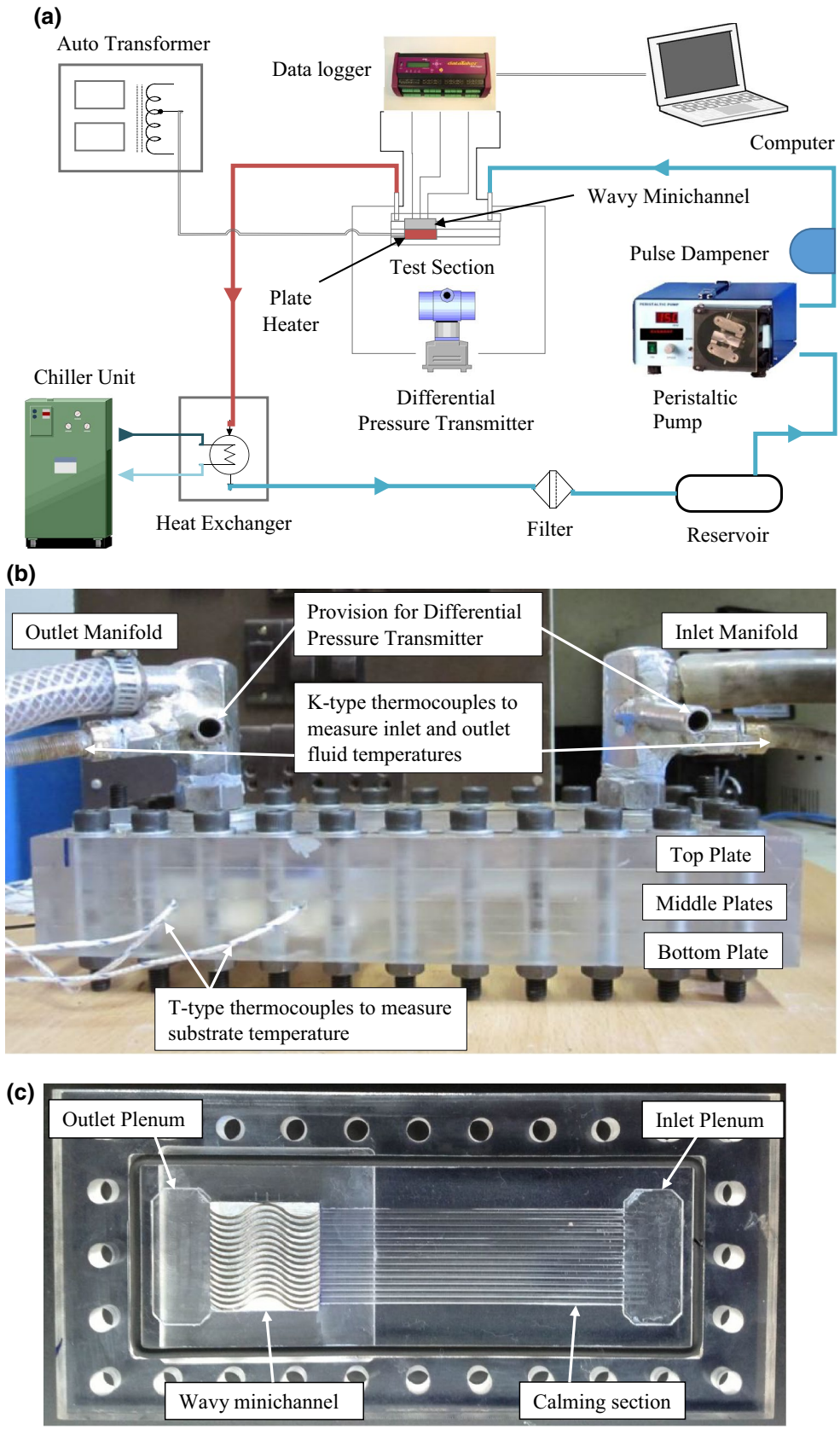

Fig. 4 **a** Schematic diagram of the experimental setup, **b** photographic side view of the minichannel heat sink assembly and **c** photographic top view of the minichannel placed in the middle plate of heat sink assembly

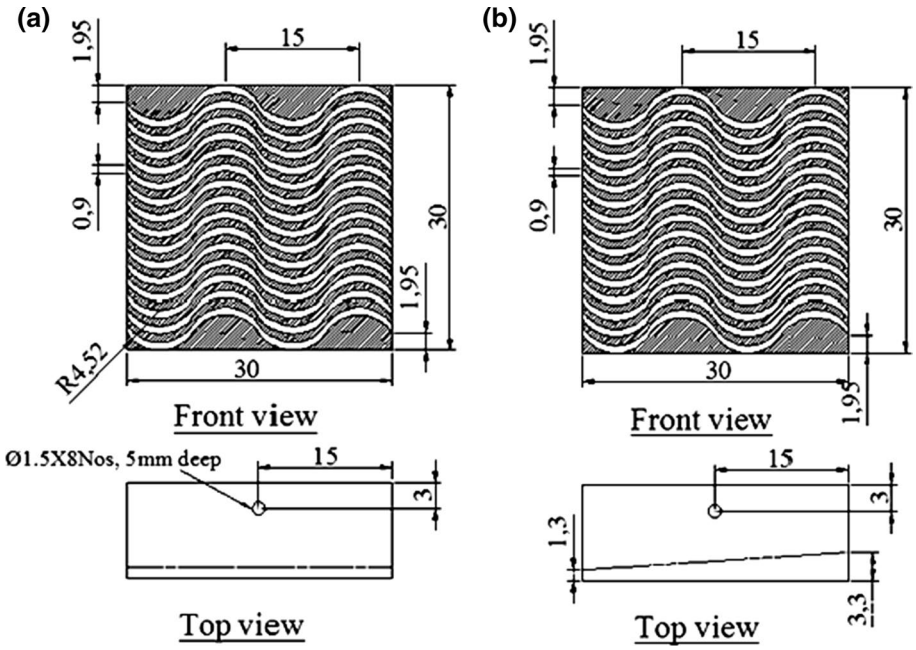

Fig. 5 Schematics of **a** constant cross-sectional wavy minichannels and **b** divergent wavy minichannels

Fig. 6 Photographic view of wavy minichannels

of the channels was varied from 1.3 to 3.3 mm with the same width of 0.9 mm. Thus, the hydraulic diameter varied from 1.063 to 1.414 mm. The width (w_f) of the fin for both configurations was 0.9 mm.

T-type thermocouples were used to measure the substrate temperatures at a depth of 8 mm from the surface and axially at 5, 15 and 25 mm from the leading edge. The channel was covered by a polycarbonate sheet because of its low thermal conductivity (0.2 W/m-K) and transparency. A resistance plate heater of size 50 mm × 50 mm × 5 mm was used as a heating source for the Aluminium minichannels and contact was properly made by applying thermal grease. An autotransformer with a voltage regulator was used to maintain constant current and voltage to the heater, which was placed below the test section. The average fluid temperatures were measured to be between 31.58 and 35.85 °C. Channel surface roughness was calculated by a profilometer and the value of surface roughness (ε) was found to be 40.94 μm.

The test section in the experimental setup was designed in such a way as to create hydrodynamically developed and thermally developing flow to increase the heat transfer rate. When the fluid enters the channel, the hydrodynamic boundary layer starts to grow from the walls. After the fluid flows for a certain distance called the entrance length, the hydrodynamic boundary layer becomes fully developed meaning that the velocity profile does not vary along the flow direction. This is similar for the thermal boundary layer also. In the experiment, the fluid was allowed to flow through a calming section whose length was higher than the hydrodynamic entrance length such that it became hydrodynamically fully developed. And then it was passed through the minichannel heat sink where a constant heat flux was given. Hence, the thermal boundary layer started developing but did not get fully developed because the length of the channel was lesser than the thermal entrance length.

3.2 Experimental uncertainties

Uncertainties analysis was carried out by using the Coleman and Steele method [32] and ANSI/ASME standard [33] to find the influence of experimental parameters on measurement variables. The uncertainties associated with experimental data are calculated on the basis of 95 % confidence level. The maximum uncertainty in the measurement of temperature was 0.104 % and for the linear dimension, it was 1 %. The uncertainty in the measurement of mass flow rate was 0.682 % and in pressure measurements, it was

11.437 %. From the above readings, the uncertainties of Nusselt number, Reynolds number and friction factor were calculated to be in the ranges of 3.890, 3.682 and 18.80 % respectively.

3.3 Data processing

The hydraulic diameter and Reynolds number were calculated using Eqs. (5) and (6) as follows.

$$D_h = \frac{4 \times \text{cross sectional area}}{\text{wetted perimeter}} \tag{5}$$

$$\text{Re} = \frac{u \times \rho \times D_h}{\mu} \tag{6}$$

The heat transfer performance of the fluids is defined in terms of convective heat transfer coefficient or Nusselt number using Eqs. (7), (8) and (9). From the pressure drop measured between the inlet and outlet plenums and other known factors [25], the apparent friction factor is calculated using Eq. (10). The apparent pressure drop is calculated by Eqs. (11) and (12).

$$Nu = \frac{hD_h}{k} \tag{7}$$

$$h = \frac{Q}{A_s(T_s - T_f)} \tag{8}$$

$$Q = mC_p\Delta T \tag{9}$$

$$\Delta P_{total} = \frac{\rho u^2}{2\left[2k_{90}\left(\frac{A_c}{A_p}\right)^2 + (k_c + k_e) + \frac{4f_{app}l}{D_h}\right]} \tag{10}$$

$$\text{Apparent friction factor,} \quad f_{app} = \frac{\Delta P_{app} D_h}{2\rho L u^2} \tag{11}$$

$$\text{Constricted diameter} \quad D_{c,f} = D_h - 2\varepsilon \tag{12}$$

4 Results and discussions

4.1 Heat transfer rate of wavy channels

4.1.1 Effect of divergent wavy form

The wavy feature of wavy minichannels increases the heat transfer rate and pressure drop compared to conventional straight minichannels [11]. Further, the higher relative waviness (A/λ) increases the heat transfer rate as well as the pressure drop [15–17]. There are three passive techniques [34] that enhance heat transfer rate in single phase flow viz. (1) Decreasing the thermal boundary layer thickness, (2) Increasing the disruption in the fluids [9, 10, 35], (3) Increasing the velocity gradient near the heat transfer wall.

When flow occurs in a wavy passage, the streamlines of the flow get disturbed [14–17]. This interruption increases mixing of the flow and thereby the heat transfer rate also increases. The regions of maximum amplitude in a wavy channel generate vortices and secondary flows. These vortices and secondary flows disturb the boundary layer growth and will not allow the flow to fully develop. The centrifugal force acting in the curvature of the channel increases pressure near the outer concave wall, thereby increasing the pressure gradient towards the centre of the flow. Due to this pressure gradient, the high-pressure fluid from the outer region moves towards the core [18, 19]. Hence secondary flow occurs, which leads to more mixing and heat transfer. However, all these mechanisms increase not only the heat transfer rate but also the pressure. In order to reduce the pressure drop of the channel, the flow passage was made divergent instead of a constant cross-section. The experimental results of wavy minichannels with constant and divergent cross-sections were compared, using DI water and Al_2O_3/water nanofluids as working fluids. Figure 7 shows the variations of Nusselt number as a function of Reynolds number. For this study, wavy channels with a relative waviness (A/λ) of 0.0667 were taken.

There are two sets of curves in Fig. 7 in which the lower set of curves represent the variations of Nusselt number as a function of Reynolds number for the wavy minichannels with constant cross-section. The other set of curves represents that of the wavy minichannels with divergent flow passage. It was observed from Fig. 7 that in the Reynolds number range between 700 and 1500, there was a 10–12 % increase in Nusselt number for every 200 increase in Reynolds number when DI water was the working fluid. And the Nu increased by 22 % for an increase in Re from 1500 to 1800, due to the change of flow from laminar to transition regime. This sudden increment in Nusselt number was due to the flow having single frequency, double frequency and more chaotic advection in turbulent region. The same trend was also observed in the friction factor curves. The curves of friction factor had a negative slope from a Re of 700–1500. But, there was a sudden increase in friction factor in the Re range from 1500 to 1800. This sudden increment showed the transition of flow. In the laminar region, the increase in Nusselt number for wavy minichannel with divergent flow passage was 9 % higher than wavy minichannel with constant cross-section. When the Re was higher than 1800, the increase in Nu was 3–5 %. The flow velocity in the channels of constant cross-section was constant along the length of the channel but decreased along the length of the divergent channel because of the gradual increase in cross-sectional area. This decelerated flow created less fullness and an adverse pressure gradient [20]. In

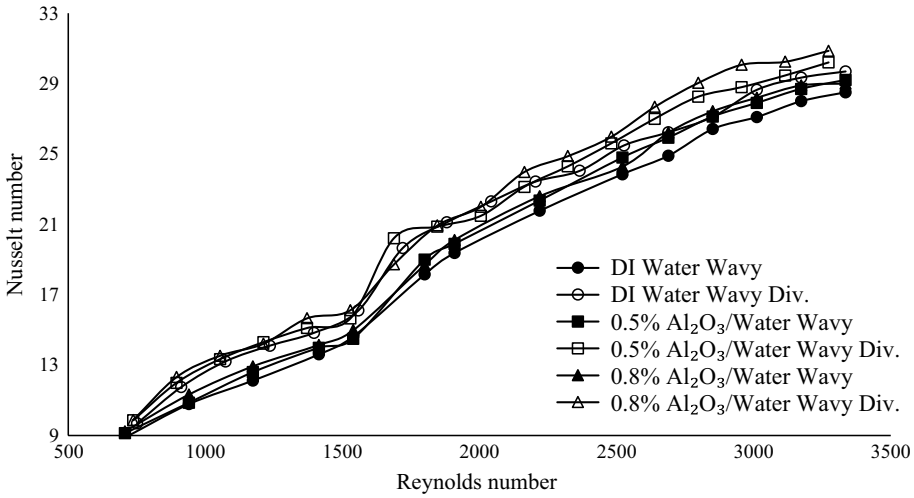

Fig. 7 Variation of Nusselt number as a function of Reynolds number

addition, it created a velocity gradient towards the center of the flow that induced more mixing and turbulence. When flow passed through the divergent passage, kinetic energy was converted into pressure energy by the conservation of energy. Outside the boundary layer, the pressure increased in the direction of flow. Hence, a part of the flow that was in the outer region of boundary layer moved in the reverse direction. This reversed flow lifted the boundary layer away from the surface. This phenomenon is known as boundary layer separation [36]. Vortices were formed in a line due to pressure gradient known as a vortex sheet. On either side of the vortex sheet, the fluid was moving in opposite direction. These vortices were inherently unstable and caused severe turbulence and mixing. The destabilization effect of the adverse pressure gradient facilitated the interaction between neighboring fluid elements and vortices that made the flow highly unsteady near the exit. This turbulence moved towards the entrance when the velocity was increased thereby reducing the temperature gradient of the flow gradually [13, 14]. Thus, this effect increased the heat transfer rate.

The temperature distribution of the heat sink gives a measure of heat transfer. The average heat transfer coefficient or the average Nusselt number shows the heat transfer performance of a system. If heat sinks distribute the heat in an improper way, hot spots will be generated that would result in the failure of components. The temperature distribution of heat sink is given by the temperature difference ($T_s - T_f$) between heat sink and fluid in the flow direction. There was no significant change in the temperature distribution of divergent wavy minichannels over those with constant cross-section.

4.1.2 Effect of nanofluids

The enhancement in the heat transfer characteristics of nanofluids is due to Brownian motion, liquid layering at liquid–particle interface, phonon movement in nanoparticles and nanoparticles clustering [6]. On increasing nanoparticles volume concentration, both thermal conductivity and viscosity will increase. But, the increase in viscosity of nanofluids was much more effective on heat transfer enhancement than the thermal conductivity for volume concentrations higher than 1 % [5]. The effect of nanofluids on the heat transfer rate was similar to that of DI water in both the regimes. In the laminar regime, the increment in heat transfer rate was 1–2 % and 2–5 % for 0.5 % and 0.8 % volume concentration Al_2O_3/water nanofluids over DI water respectively in the divergent wavy channels. Thus, it can be seen that nanofluids have a less significant effect on heat transfer than the change in channel geometry. In the case of wavy channels, secondary flow (Dean Vortices) develops when liquid coolant passes through the wavy geometry. The pattern of Dean Vortices may change significantly along the flow direction, which can lead to chaotic advection, thus greatly enhancing convective fluid mixing and heat transfer [10].

However, when the Re was higher than 1500, Nusselt number of nanofluids converges to that of water. This is due to the suppression of transport behavior of nanoparticles in the turbulent regime [7]. The average flow temperature of nanofluids was higher than that of DI water [5, 6]. At the advent of the transient regime, the trend of a sudden increase in Nusselt number was similar to that of DI water. A similar behavior was also noticed in the constant cross-section wavy minichannels. Nanofluids showed better results in the laminar regime than in the turbulent regime [5–7]. It is also seen in literature that the performance of nanofluids converges to that of the base fluid in the turbulent regime [7]. Despite the lower specific heat, increased volume concentration of nanoparticles increased the surface and fluid temperatures [6, 21].

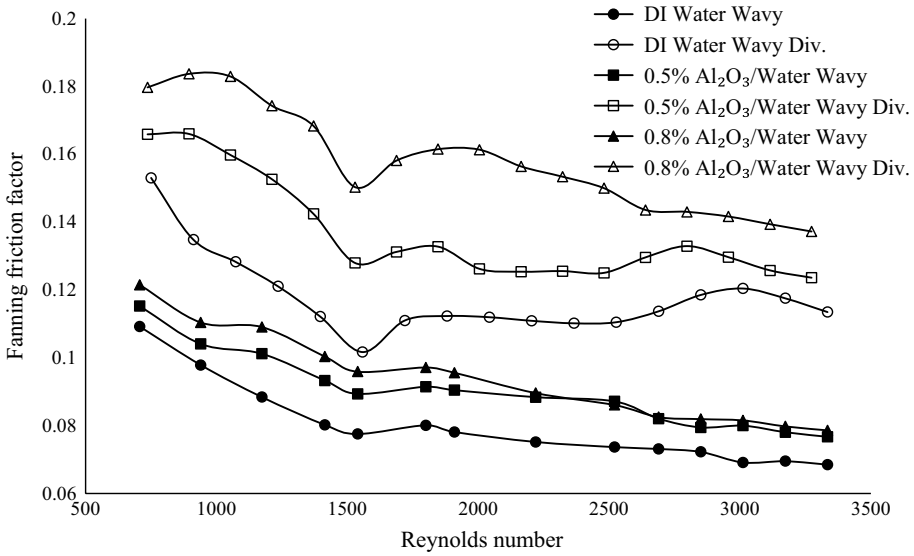

Fig. 8 Fanning friction factor as a function of Reynolds number

4.2 Friction factor and pressure drop

The differential pressure between the inlet and exit manifold of the experimental setup was measured using a differential pressure transmitter in the absence of heat flux. The output value represents the total pressure drop which includes the effect of the losses in bends, entrance and exit losses, developing region effects, and the core (apparent) frictional losses. The apparent friction factor [8] was found using Eq. (10). The apparent pressure drop was obtained from the experimental results by using Eq. (11).

4.2.1 Friction factor

From the experimental results shown in Fig. 8, the trend of a decrease in friction factor with an increase in Reynolds number continued up to around Re 1500. The transitioning of the flow happened around the Reynolds number range between 1500 and 1800. It was slightly earlier than that predicted by conventional theories. But this kind of earlier transition had been noticed by many researchers [8–10]. The reason for this earlier transition is increased relative waviness and relative roughness of the flow surface [8]. Then the friction factor increased for some extent and then was steady thereafter. The friction factor of the divergent wavy channel was 40–59 and 50–64 % higher in laminar and transient regimes respectively than that of the constant cross-sectional wavy channels for DI water. This was due to increased surface area and decelerated flow in the divergent channel. The trend was similar in the constant cross-section channels.

Nanofluid increases fluid friction because of higher shear stress or viscosity and density. Increasing concentration of nano particles increases fluid friction. Flow in divergent wavy minichannels showed an increased friction factor of 43–75 and 45–90 % in laminar and transient regimes respectively over constant cross-section wavy minichannels using 0.5 and 0.8 % volume concentration of nanofluids. In the transient regime, the friction factor of water was almost constant, but decreasing for nanofluids. This was because small particles suppressed turbulence by acting as an additional source of dissipation. Since we used 40 nm diameter nano particles and Reynolds number was less than 3500, the particles used were considered small [18].

4.2.2 Pressure drop

Flow disruption is one of the best techniques to enhance convective heat transfer. However, flow disruption will simultaneously increase the pressure drop, which in turn causes mechanical stress, component failure, high pumping power etc. To conquer these problems, flow in a divergent passage was investigated. In the case of flow in a divergent wavy channel, the pressure drop is lower but the friction factor is higher than those for a constant cross-section wavy channel. As discussed for the heat transfer, flow in the divergent channel caused a part of the kinetic energy to be converted into pressure energy. This increased static pressure leads to a reduced pressure drop. Also, the friction factor is higher because of the combined effect of increased flow area, decelerated flow and the destabilizing effect [18–20]. Figure 9 shows the experimental variation of pressure drop as a function of Reynolds number. The pressure drop was 30–38 % lower in the laminar regime and an average of 45 % lower in the transient regime compared to constant cross-sectional minichannels when DI water was the working fluid.

The effect of nanofluids on pressure drop reduction was similar to that of DI water. The pressure drop for 0.5 and

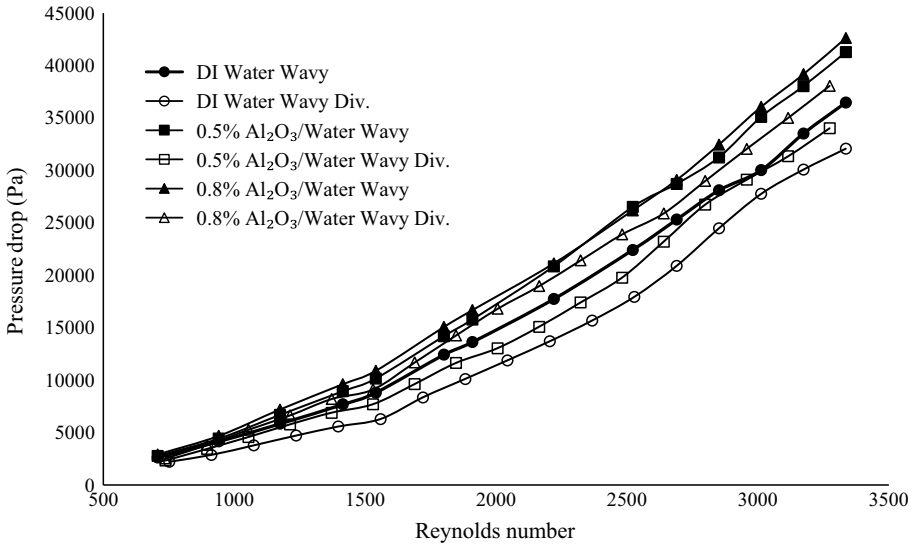

Fig. 9 Variation of Pressure drop as a function of Reynolds Number

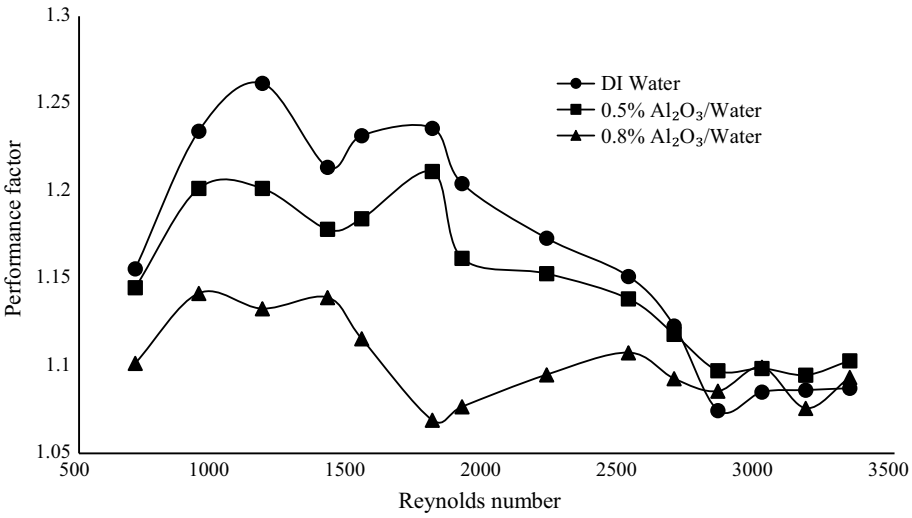

Fig. 10 Performance factor as a function of Reynolds number

0.8 % volume concentrations of Al_2O_3/water nanofluid was 22–38 and 26–38 % lower in the laminar region of divergent minichannels than the constant cross-sectional minichannels respectively. Similarly, an average reduction in pressure drop of 45 % for 0.5 % nanofluid and 35 % for 0.8 % nanofluid was observed in the transient regime.

4.3 Overall performance factor (PF)

To check the performance of divergent passages, the heat transfer performance of the two wavy channel configurations is compared along with the pressure drop. The hydraulic diameters of the channels in the two heat sinks were not the same. The angle of divergence of the divergent wavy minichannels being 3.81°, varied the hydraulic diameter. Figure 10 shows Performance Factor (PF) as a function of Reynolds number. It was calculated from Eq. (13) [37, 38].

$$PF = \frac{Nu_{WavyDiv} / Nu_{Wavy}}{\left(\Delta P_{WavyDiv} / \Delta P_{Wavy}\right)^{1/3}} \tag{13}$$

The PF was greater than one for divergent wavy minichannels because of a higher rate of mixing, more time, space and reduced pressure drop. It is evident from Fig. 10 that the performance factor for water increased from 1.15 to 1.26 in the laminar regime but it decreases to 1.08 in the transient regimes. The trend of PF of nanofluids was the same, but it was 1.14–1.2 for 0.5 % volume concentration and 1.1–1.13 for 0.8 % volume concentration of Al_2O_3/water nanofluid respectively in the laminar regime. This was due to increased density, momentum and viscosity of nanofluids, which increased wall shear stress, heat transfer performance as well as pressure drop. In the transient regime, the PF of DI water and nanofluids

converged to 1.08. This is because the effect of nanofluids was suppressed [18] by chaotic mixing in the wavy minichannels.

5 Conclusion

The heat transfer and pressure drop characteristics of divergent wavy minichannels were studied. The flow was single phase forced convective, hydrodynamically fully developed and thermally developing. From this experimental investigation, the following conclusions have been made:

- The enhancement in Nusselt number due to channel divergence was 9 % in the laminar regime and 3–5 % in the transient regime using DI water, due to an increased surface area and increased height to width ratio.
- The enhancement in Nusselt number due to nanofluids in divergent wavy minichannels was 1–2 and 2–5 % for 0.5 and 0.8 % volume concentrations of Al_2O_3/water nanofluid respectively in the laminar regime. In the transient regime, it reduced to 2 %, because the small particles suppressed turbulence by acting as an additional source of dissipation. The trend is similar for wavy minichannels with constant cross-section.
- Due to the channel divergence, an increase in friction factor of 40–59 and 50–64 % in laminar and transient regimes respectively was seen for DI water. This was due to increased surface area, decelerated flow and the destabilizing effect in the divergent channels. In the transient regime, the friction factor increased for some extent and then was steady. The usage of nanofluids also resulted in similar trends of friction factor.
- The pressure drop of divergent wavy minichannels was lower than wavy minichannels by 30–38, 22–38 and 26–38 % in the laminar regime and by 45 % in the transient regime for DI water, 0.5 and 0.8 % volume concentrations of Al_2O_3/water nanofluids respectively. This is due to increased diameter and reduced velocity of flow in the divergent flow passage. Divergent flow is one of the better ways to reduce pressure drop.
- The performance factor for flow in the divergent wavy minichannels over constant cross-section wavy minichannels was 1.15–1.26 for water and 1.1–1.13 for nanofluids. The reduction in performance factor for nanofluids is due to its higher density, viscosity and friction factor.
- Nanofluids were well dispersed and in excellent stable condition. There was no clogging, sedimentation and erosion because of the low concentration of nanofluids (less than 1 %) [5, 6].

Hence, divergent wavy minichannel heat sinks offer two advantages over constant cross-section wavy minichannel heat sinks: a better heat transfer performance and a reduced pressure drop. Nanofluids offer a slightly higher heat transfer performance over DI water in divergent wavy minichannels, but with an increased pressure drop.

References

1. Mehta B, Khandekar S (2012) Infra-red Thermography of laminar heat transfer during early thermal development inside a square mini-channel. Exp Thermal Fluid Sci 42:219–229
2. Lee PS, Garimella SV, Liu D (2005) Investigation of heat transfer in rectangular micro channels. Int J Heat Mass Transf 48:1688–1704
3. Ho CJ, Wei LC, Li ZW (2010) An experimental investigation of forced convective cooling performance of a microchannel heat sink with Al_2O_3/water nanofluid. Appl Therm Eng 30:96–103
4. Jung JY, Oh HS, Kwak HY (2009) Forced convective heat transfer of nanofluids in microchannels. Int J Heat Mass Transf 52:466–472
5. Sahin B, Gültekin G, Manay E, Karagoz S (2013) Experimental investigation of heat transfer and pressure drop characteristics of Al_2O_3—water nanofluid. Exp Therm Fluid Sci 50:21–28
6. Lee J, Mudawar I (2007) Assessment of the effectiveness of nanofluids for single-phase and two-phase heat transfer in microchannels. Int J Heat Mass Transf 50:452–463
7. Liu D, Yu L (2011) Single-phase thermal transport of nanofluids in a minichannel. J Heat Transf ASME 133(3):031009
8. Soban CB, Peterson GP (2012) Microscale and nanoscale heat transfer. ISBN 978-0-8493-7307-7
9. Steinke ME, Kandlikar SG (2004) Single-phase enhancement techniques in micro channel flows. ASME ICMM 2004:2328
10. Garimella SV, Singhal V (2004) Single-phase flow and heat transport and pumping considerations in micro channel heat sinks. Heat Transf Eng 25(1):15–25
11. Dominic A, Sarangan J, Suresh S, Devah Dhanush VS (2015) An experimental investigation of wavy and straight minichannel heat sinks using water and nanofluids. J Therm Sci Eng Appl 7(3):031012
12. Salman BH, Mohammed HA, Munisamy KM, Kherbeet AS (2013) Characteristics of heat transfer and fluid flow in microtube and microchannel using conventional fluids and nanofluids: a review. Renew Sustain Energy Rev 28:848–880
13. Rush TA, Jacobi AM, Newell TA (1999) An experimental study of flow and heat transfer in wavy passages. Int J Heat Mass Transf 42:1541–1553
14. Nishimura T, Kajimoto Y, Tarumoto A, Kawamura Y (1986) Flow structure and mass transfer for a wavy channel in transitional flow regime. J Chem Eng Jpn 195:449–455
15. Sui Y, Teo CJ, Lee PS (2012) Direct numerical simulation of fluid flow and heat transfer in periodic wavy channels with rectangular cross-sections. Int J Heat Mass Transf 55:73–88
16. Sui Y, Teo CJ, Lee PS, Chew YT, Shu C (2010) Fluid flow and heat transfer in wavy microchannels. Int J Heat Mass Transf 53:2760–2772
17. Sui Y, Lee PS, Teo CJ (2011) An experimental study of flow friction and heat transfer in wavy microchannels with rectangular cross section. Int J Therm Sci 50:2473–2482
18. Yang CS, Jeng DZ, Liu CW, Liu CG, Gau C (2010) Fluid flow and heat transfer in a horizontal channel with divergent top wall and heated from below. J Heat Transf 132(8):081403
19. Liu CW, Gau C (2004) Onset of secondary flow and enhancement of heat transfer in horizontal convergent and divergent channels heated from below. Int J Heat Mass Transf 47:5427–5438

20. Shah MK, Tachie MF (2008) PIV Study of turbulent flow in asymmetric converging and diverging channels. J Fluids Eng 130:011204-1–01120401120401120415
21. Wang LB, Tao WQ, Wang QW, Wong TT (2001) Experimental study of developing turbulent flow and heat transfer in ribbed convergent/divergent square ducts. Int J Heat Fluid Flow 22:603–613
22. Dominic A, Sarangan J, Suresh S, Devah Dhanush VS (2014) An experimental study of forced convective fluid flow in divergent minichannels using nanofluids. Appl Mech Mater 592:1418–1422
23. Kandlikar SG (2012) History, advances, and challenges in liquid flow and flow boiling heat transfer in microchannels: a critical review. J Heat Transf 134(3):034001
24. Ghadimi A, Saidur R, Metselaar HSC (2011) A review of nanofluid stability properties and characterization in stationary conditions. Int J Heat Mass Transf 54(17):4051–4068
25. Pak BC, Cho Y (1998) Hydrodynamic and heat transfer study of dispersed fluids with submicron metallic oxide particle. Exp Heat Transf 11:151–170
26. Xuan Y, Roetzel W (2000) Conceptions for heat transfer correlation of nano fluids. Int J Heat Mass Transf 43:3701–3707
27. Einstein A (1956) Investigation on the theory of Brownian motion. Dover, New York
28. Maxwell JC (1954) Treatise on electricity and magnetism. Dover, New York
29. Suresh S, Venkitaraj KP, Selvakumar P, Chandrasekar M (2012) Effect of Al2O3–Cu/water hybrid nanofluid in heat transfer. Exp Therm Fluid Sci 38:54–60
30. Chandrasekar M, Suresh S, Bose AC (2011) Experimental studies on heat transfer and friction factor characteristics of Al_2O_3/water nanofluid in a circular pipe under transition flow with wire coil inserts. Heat Transf Eng 32(6):485–496
31. ISO/TC24 (1996) ISO 13321:1996, Particle size analysis - photon correlation spectroscopy. International Organization for Standardization, Geneva, Switzerland
32. Steele WG, Coleman HW (1989) Experimental and uncertainty analysis for engineers. Wiley, New York
33. ANSI/ASME (1986) Measurement uncertainty. PTC 19, 1–1985, ASME, New York
34. Tao WQ, He YL, Wang QW, Qu ZG, Song FQ (2002) A unified analysis on enhancing single phase convective heat transfer with field synergy principle. Int J Heat Mass Transf 45:4871–4879
35. Anandan SS, Ramalingam V (2008) Thermal management of electronics: a review of literature. Therm Sci 12(2):5–26
36. Nakayama Y, Boucher RF (1999) Introduction to fluid mechanics. ISBN 0 340 67649 3
37. Gee DL, Webb RL (1980) Forced convection heat transfer in helically rib-roughened tubes. Int J Heat Mass Transf 23:1127–1136
38. Gong LJ, Kota K, Tao W, Joshi Y (2011) Thermal performance of microchannels with wavy walls for electronics cooling. IEEE Trans Compon Packag Manuf Technol 1(7):1029–1036